Experiments, Modelling, and Simulations for a Gel Bonded to a Rigid Substrate

Sichen Song[1,2] · Ronald A. Siegel[1] · Manuel A. Sánchez[3] · M. Carme Calderer[2] · Duvan Henao[4,5]

Abstract

In preparation for a more thorough study based on our own experimental work of the debonding of a thin film gel by stress concentration on the interface with a rigid substrate, in this article we revisit, from the viewpoint of the synergy between mathematics, experiments, and finite element simulations, the problem of the swelling of a thin rectangular polyacrylamide gel covalently bonded on the bottom surface to a glass slide. With methods of the calculus of variations and perturbation theory we show that the solution to the corresponding zero-displacement boundary value problem converges, in the thin film limit, to a uniquely defined uniform uniaxial extension on the direction normal to the substrate. Both the experiments and the finite element simulations that we perform confirm that the amount of lateral swelling is very small, with a very good quantitative agreement between the two approaches. The proposed model of minimizing an energy functional comprising both a term for the elastic distortion and the Flory-Huggins expression for the entropy of mixing is thus experimentally and numerically validated, with parameters coming from experimental measurements, including the initial polymer volume fraction of the hydrogel synthesized in the laboratory (which is taken as the reference configuration instead of the dry polymer).

1 Introduction

The present article builds upon the variational model proposed by Calderer, Garavito, Henao, Tapia & Lyu [9] for the debonding of a gel from a rigid substrate. The goal is to aid in the design of the synthetic polymers that coat a pacemaker, or other medical implants, by determining how thin the gel coating ought to be in order for it to be stable against debonding from the mechanical substrate. This challenging task needs to take into account the curvature of the substrate; the nature of the adhesion between the gel film and the substrate; the entropic gain due to the absorption of water from the high moisture environment of the body, and the geometry and topology of the debonded regions of the gel/substrate interface, among others.

Extended author information available on the last page of the article

In [9] a simplified, essentially two-dimensional setting, was considered, as a first step. The advantage of the simplified problem is that it yields a closed-form formula for the threshold thickness for stability against debonding (see Sect. 3.8 for a more detailed explanation). The explicit nature of this formula makes it potentially valuable in medical device development.

The underlying simplifying assumptions are incompatible with a curved substrate, truly three-dimensional expansions, rate-dependent debonding, curved debonding fronts, and multiple debonded regions of the gel/substrate interface. This article goes a step further in this program. First, we perform free-swelling and fully-bonded experiments with poly-acrylamide gel, in light of which the variational model is adjusted and the distance between the actual three-dimensional expansion and the idealized thin-film-limit uniaxial solution is measured. Second, we perform finite element simulations, obtaining a more thorough comparison between the model and the experiments in the laboratory. Regarding the improvements on the model due to the understanding from the experimental work and the numerical simulations: (a) now all the parameters are obtained from experimental measurements; (b) the reference configuration is taken with the physical initial polymer volume fraction ϕ_0 and the shear modulus is that of the synthetized hydrogel (instead of working with $\phi_0 = 1$ and the shear modulus of the dry polymer), and (c) the thin film asymptotic analysis is now made for the full 3D problem (instead of working with a class of deformations where swelling is possible only in the vertical direction and in one of the horizontal directions, as is done in [9]). Regarding the agreement between the experimental observations, the thin film theoretical prediction for the vertical stretch in the bonded sample, and the finite element solutions, the results are encouraging and might motivate new research on this rich mechanical/gel polymer physics problem.

This work strongly relies on the natural synergy between mathematics and experiments, and how they inform each other throughout the course of the work. In particular, the experimental measurements combined with the model have contributed to determining the value of the Flory-Huggins parameter χ and the shear modulus of the gel under investigation. A message for a mechanician is to reassess the role of the choice of the reference configuration of the problem. In many works on gels, including [9], the reference configuration is chosen to be that of the dry polymer, that is, with $\phi_0 = 1$. However, a consistent experimental set up would require a large energy expense to arrive at such a goal. The finite element simulation of the model shares some analogies with a previous study of gel equilibrium by the method of mixed finite elements, involving a related but different equilibrium model than the present one. No experimental work was directly associated to that analysis [28].

We now include a brief survey of gel research to illustrate the highly interdisciplinary nature of the field, fully aware that justice will not be served to the many important contributions of past and current researchers. Many of the current approaches to modeling gels rely in great part on the theory of mixtures of two components, a polymer network and solvent, specifically in the form of poroelasticity. With its origins in the prominent work by Biot [5], it played a prominent role in geophysics, in connection with the problem of extraction of oil from the earth substrates, and, in particular, driving the development of analysis and numerical methods for such systems [2]. Research on mixture theory from the point of view of continuum mechanics was simultaneously carried out by the group of Ericksen and Truesdell in Johns Hopkins University, with many of such contributions reported in the volume by Truesdell and Noll [32]. In particular, these authors contributed to making precise some fundamental concepts in mixture models, and making their mathematical formulations precise. One such instance is the concept of a mixture with incompressible constituents, where each isolated individual component is incompressible. However, while the Jacobian of such

deformations of such a material in a separate setting has value one, this is not the case in a mixture. The 'averaged material' does sustain deformations with determinant larger than one. (In the case of polyelectrolyte gels, such a Jacobian can be larger than 500.) The situation is very different in geophysical mixtures that are genuinely compressible, since they involve individual components, such as natural gas, with that property. As a result, a general well-posedness theory of compressible mixtures is lacking.

The works by the Ericksen and Truesdell's group on mixture theories mostly deal with fluid components, with the treatment of solid-liquids being pursued afterwards by several authors in that community, starting with linearized elasticity models for the solid component. Works in this direction include those of Bowen [8], Weinman & Rajagopal [34], and Pence [26].

As many authors, including de Gennes, Doi, and Tanaka, have made clear, a gel is not a poroelastic material in its strict sense (as one could think, for instance, of a sponge), since chemical interactions among the components are essential for the new material, the gel, to arise. This motivates us to bring forward the studies of interacting polymer and solvent mixtures by Flory and Huggins ([15], [20]) and Flory and Rehner [16], focused on the study of gels. Tanaka and Fillmore published a leading article on the kinematics of gels, based on linear elasticity but with emphasis on the non-diffusive nature of the swelling regimes [31]. Doi later incorporated nonlinear elasticity and focused on the volume phase transition caused by swelling-collapse processes. A gel monograph by this author gives a very clear perspective of the status of the research of gel mechanics up to date [14]. A full incorporation of nonlinear elasticity with the Flory theory was promoted in the articles by Suo and co-authors, with models closely developed alongside experiments [6, 19, 21, 33]. In particular, with the aim of removing the limitations of the linear approaches, they suggested a new procedure to fit the experimental data with the nonlinear theory. Furthermore, they proposed an indentation experiment as an effective method for characterizing the mechanical and transport properties of polymer gels. Work by the latter authors also addresses surface instabilities in gel, with examples of cavitation presented in the work of Pence [27] and fibrillation by Doi [14]. See also the work by Mora & Boudaoud [23] on the formation of wavy periodic patterns in thin soft gels clamped to a stiff gel. Another challenge in the mathematical treatments of gels is the role of the boundary conditions, either in free swelling or under confinement. In both cases, one has to take into account the permeability properties of the gel boundary, ranging from fully permeable, semi permeable or impermeable [10]. In confinement, gels may develop stress concentrations on the boundary leading to possible debonding from the substrate [9]. Although not immediately related to the topic of the current article, polylelectrolyte gels make a primary field of gel research. With the prominent role of the chemical interaction between components, the role of ions in the vicinity of charged polymers gives the materials outstanding properties such as swelling ratios above 500. Models of such gels required the coupling of mechanical equations with those of Poisson-Nernst-Planck type [24]. The electro-mechanical coupling also presents the opportunity for a myriad of devices. An example can be found in a rhythmic drug delivery device, powered by glucose, that harnesses swelling-collapse transitions [4, 13, 22, 35].

The present article is organized as follows. Section 2 is devoted to the description of the gel experiments and the materials used. In Sect. 3, we present the model, including the formulation of the energy, the setting of the stress tensor, and the derivation of uniform, energy minimizing solutions, including the free swelling and the partially bonded configurations. At this point, we have gathered sufficient information so that, combining the model with the experimental results, we calculate the Flory-Huggins parameter χ of the gel. We continue with the formulation of the boundary value problems in three space dimensions and obtain

the thin film limit, result that to the best of our knowledge, is obtained here for the first time. Section 4 is devoted to the finite element simulation of the solutions of the boundary value problems, emphasizing the quantitative connections with the experiments. In Sect. 5, we draw some conclusions.

2 Experimental Section

2.1 Materials

Acrylamide (AAm, A8887; Sigma-Aldrich, St. Louis, MO), N,N-methylenebisacrylamide (MBAA, 146072; Sigma-Aldrich, St. Louis, MO), ammonium persulphate (APS, A3678; Sigma-Aldrich, St. Louis, MO), N,N,N',N'-tetramethylethylenediamine (TEMED, T9281; Sigma-Aldrich, St. Louis, MO), functional silane 3-(trimethoxysilyl) propyl methacrylate (TMSPMA, 440159; Sigma-Aldrich, St. Louis, MO), acetic acid (VWR International LLC., Radnor, PA), ethanol (EtOH; VWR International LLC., Radnor, PA), and acetone (Fisher Chemical, Fair Lawn, NJ) were used as received.

2.2 Methods

2.2.1 Preparation of Polyacrylamide (PAAm) Gel

PAAm gels were synthesized by vortexing 10 mL degassed (dry N_2 purging for 10 min) aqueous precursor solution (2.3 g AAm, 5.1 mg MBAA, and 4.3 mg APS) with 10 μL TEMED, quickly pouring the mixture into laser cut acrylic molds with specified shapes, covering with pre-cleaned glass plates, and keeping it overnight for stabilization.

The volume fraction occupied by the polymer phase in the resulting hydrogels was approximately

$$\phi_0 = 0.2035. \tag{1}$$

2.2.2 Free Swelling Experiment

Rectangular PAAm gels (length: 90.0 mm, thickness: 3.0 mm, width: 23.5 mm) were immersed in deionized (DI) water (frequently changed to remove extra chemicals) for 10 days (after which was at swelling equilibrium). The length, width, and thickness of the gels at equilibrium were measured with a digital caliper (General Tools & Instruments, Andover, MN). All the experiments were carried out at $T = 296$ K.

2.2.3 Swelling of a Completely Bonded Gel

Rectangular gels (length: 90.0 mm, thickness: 1.62 mm, and width: 15.0 mm) were completely covalently anchored on glass substrates following the procedure of Sect. 2.2.4. They were immersed in DI water (changed three times) for around 72 hours to reach swelling equilibrium. Dimensions in the equilibrium state were measured using the same digital caliper.
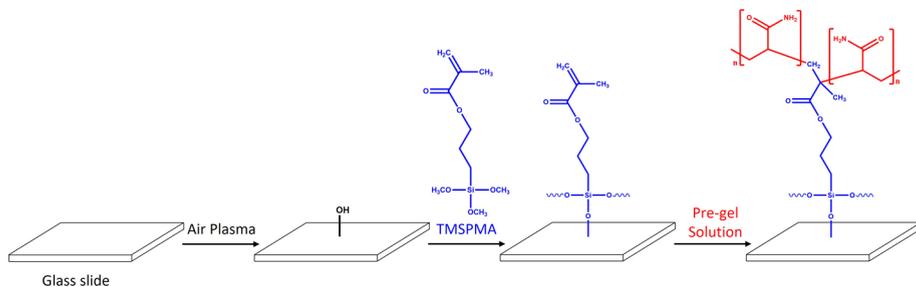
Fig. 1 Illustration of covalent bonding of the PAAm gel to a glass slide

2.2.4 Gel Anchoring on a Glass Substrate

Gels were chemically anchored on a glass substrate following a protocol from reference [36]. Briefly, surfaces of glass slides were functionalized by grafting functional silane TMSPMA. Glass slides were thoroughly cleaned with acetone, ethanol, and DI water, and were then completely dried. Cleaned glass slides were treated with air plasma (50 W under a pressure of 300 mtorr; Plasma Etch Inc., Carson City, NV) for 5 min. Immediately after the air plasma treatment, the glass surface was covered with silane solution (100 mL DI water, 10 μL acetic acid with pH=3.5, and 2 mL TMSPMA), and incubated for 2 hours. Glass slides were washed with ethanol and completely dried. Functionalized substrates were stored in a 0% RH desiccator before use. The procedure is illustrated in Fig. 1.

2.2.5 Elastic Modulus (G)

Mechanical properties of disk shaped (diameter: 25 mm, thickness: 6.3 mm) PAAm gels were determined under amplitude oscillation mode using an RSA-G2 solids analyzer with a parallel plate (diameter: 25 mm) geometry (TA Instruments, New Castle, DE). Each gel was placed on the bottom plate after zero gap calibration. Dynamic storage and loss moduli were measured with oscillation strain 0.01%–1% and fixed angular frequency 1 rad/s with baseline compression of approximately 10 g. Measurements were completed within 2 minutes to avoid any redistribution of water inside the gel.

2.3 Results

2.3.1 Free Swelling Experiment

The dimensions of the gel at swelling equilibrium, in three repetitions of the experiment, are presented in Table 1. In the three repetitions a homogeneous deformation was observed, with stretches given approximately by 1.49, 1.49, and 1.48 (along the length, thickness, and width directions, respectively). This was very close to the isotropic expansion with a Jacobian determinant of 3.29 (the factor by which the volume of the gel increased in each of the repetitions of the experiment).

2.3.2 Swelling of a Completely Bonded Gel

For the gel completely bonded to a glass slide, the experiment was repeated four times. The deformation reached after swelling was close to a homogeneous uniaxial extension, normal

Table 1 The Jacobian determinant J is the ratio between the volume at the swelling equilibrium and the volume of the reference configuration. It gives the increased volume factor for each of the three repetitions of the experiment. The average Jacobian is 3.2908 (standard deviation 0.0068) which corresponds to a ratio of isotropic extension $\hat{\lambda}_{iso} := J^{1/3} = 1.4874$. The stretch factor presented in the table is the average, considering the three repetitions of the experiment, of the ratio L_{eq}/L_i, where L_{eq} is the dimension (length, width, or thickness) of the gel at swelling equilibrium and L_i is the corresponding dimension in the initial state

Configuration	Length (mm)	Thickness (mm)	Width (mm)	Jacobian determinant J
Reference	90.0	3.0	23.5	1
Gel 1	134.24	4.48	34.69	3.2880
Gel 2	134.49	4.47	34.68	3.2858
Gel 3	134.62	4.47	34.78	3.2985
Average	134.45	4.47	34.72	3.2908
SD	0.19	0.0058	0.055	0.0068
Stretch factor	1.4865	1.4911	1.4773	
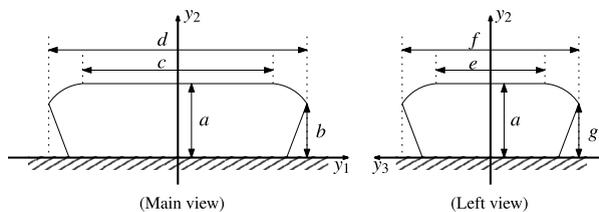
Fig. 2 Observed shape of the completely bonded gel at swelling equilibrium. The illustration exaggerates the rounding-off at the upper corners, and the outward displacement of the lateral surfaces (the actual aspect ratio d/a, in the main view, is of the order of 94 : 3, as can be seen in Table 2 and in Figure 19). The frame y_1, y_2, y_3, with the notation that will be used in the expressions $\mathbf{y} = \mathbf{x} + \mathbf{u}(\mathbf{x})$, $\mathbf{x} = (x_1, x_2, x_3)$, $\mathbf{y} = (y_1, y_2, y_3)$ in the mathematical model, is depicted here with heavy lines in both the main and the left views (in particular, we denote the vertical direction by y_2)

to the substrate. The final thickness a, measured in the middle region of the sample; and the deviation from the idealized uniaxial extension, measured by the parameters c, d (main view) and e, f (left view) of the schematic representation of Fig. 2, are presented in Table 2.

Most of the gel was observed to swell uniformly, almost entirely in the direction normal to the glass slide. Nevertheless, detailed cross-sections show a relatively small 'bread loafing' effect, i.e., a tendency to lateral swelling that increases as one moves away from the bonding surface. The amount of lateral displacement is very similar in the two horizontal directions, close to 2 mm on each side: the difference of 3.73 mm between the measurement d and the length of 90.0 mm of the gel in its initial state, accounts for the sum of the displacements to the left and to the right of the sample; the difference of 3.95 mm between the measurement f and the initial width of 15 mm, accounts for the displacements towards the back and the front.

2.3.3 Elastic Modulus

The PAAm gel samples prepared were found to have an elastic modulus of

$$G = 0.13 \text{ MPa}. \tag{2}$$

Table 2 The table shows the parameters (in mm) a, b, c, d, e, f, and g of Fig. 2, in four repetitions of the completely bonded swelling experiment. The thickness of the sample in the middle region (parameter a) is 3.40 mm in average. The deformation is close to a homogeneous uniaxial extension, by a factor of $\hat{\lambda}_{\text{uni}} := 3.40/1.62 \approx 2.10$, in the direction normal to the glass slide

Configuration	a	b	c	d	e	f	g
Reference	1.62	1.62	90.0	90.0	15.0	15.0	1.62
Gel 1	3.31	2.05	88.08	93.90	11.42	19.00	1.75
Gel 2	3.35	2.13	88.39	93.85	11.68	18.99	1.78
Gel 3	3.50	2.01	88.31	93.56	11.49	18.79	1.72
Gel 4	3.45	2.23	88.25	93.62	11.86	19.00	1.64
Average	3.40	2.11	88.26	93.73	11.61	18.95	1.72
SD	0.09	0.10	0.13	0.17	0.20	0.10	0.06

3 Model

We assume that a gel is a saturated and immiscible mixture of elastic solid and fluid, constituents which are both assumed to be incompressible. In the reference configuration, which will be chosen to be the initial state obtained with the preparation of the rectangular PAAm gels (as described in Sects. 2.2.1, 2.2.2, and 2.2.3) the polymer occupies a domain $\Omega \subset \mathbb{R}^3$. When the samples are immersed in water, deformation of the polymer occurs by the absorption of fluid. We describe deformation by the one-to-one, differentiable map

$$\mathbf{y} = \mathbf{x} + \mathbf{u}(\mathbf{x}), \quad \text{which satisfies} \quad \det(\mathbf{I} + \nabla \mathbf{u}(\mathbf{x})) > 0, \ \mathbf{x} \in \Omega, \tag{3}$$

where $\mathbf{u} : \Omega \to \mathbb{R}^3$, $\mathbf{u}(\mathbf{x}) = \big(u_1(\mathbf{x}), u_2(\mathbf{x}), u_3(\mathbf{x})\big)$ is the displacement field and $\mathbf{I}$ denotes the 3×3 identity matrix. The domain occupied by the gel after the deformation is the image $\Omega' := (\mathbf{id} + \mathbf{u})(\Omega)$ of Ω by the deformation map $\mathbf{id} + \mathbf{u}$ (herefORTH $\mathbf{id}$ will denote the identity map, so that $\mathbf{id} + \mathbf{u}$ evaluated at $\mathbf{x}$ gives $\mathbf{y}$). We label the fluid and polymer components with indices *1* and *2*, respectively. According to the theory of mixtures, a point $\mathbf{y}$ in the current (deformed) configuration is occupied by, both, fluid and solid at volume fractions $\phi_1 = \phi_1(\mathbf{y})$ and $\phi_2 = \phi_2(\mathbf{y})$, respectively. An immiscible mixture is such that the constitutive equations depend explicitly on the volume fractions ϕ_i, $i = 1, 2$. We let ρ_i denote the mass density of the i-th component (per unit volume of deformed gel). It is related to the intrinsic density, γ_i, by the equation $\rho_i = \gamma_i \phi_i$, $i = 1, 2$. Moreover $\gamma_i = \text{constant}$, $i = 1, 2$ defines a mixture with incompressible constituents. The assumption of saturation of the mixture

$$\phi_1 + \phi_2 = 1 \tag{4}$$

expresses that no species other than fluid and polymer are present. As a consequence, it suffices to know the volume fraction of polymer, which henceforth will be denoted simply by ϕ:

$$\phi(\mathbf{y}) := \phi_2(\mathbf{y}) = \text{(swollen) polymer vol. fraction at } \mathbf{y}. \tag{5}$$

The equation of balance of mass of the polymer states that, for every subset $\tilde{\omega} \subset \Omega$,

$$\int_{(\mathbf{id}+\mathbf{u})(\tilde{\omega})} \phi(\mathbf{y}) \, d\mathbf{y} = \int_{\tilde{\omega}} \phi_0 \, d\mathbf{x}, \tag{6}$$

where $0 < \phi_0(\mathbf{x}) < 1$ denotes the volume fraction of polymer in the reference configuration. Formally, it reduces to a pointwise relation

$$\phi(\mathbf{x} + \mathbf{u}(\mathbf{x})) J(\mathbf{x}) = \phi_0(\mathbf{x}), \quad \text{for all} \quad \mathbf{x} \in \Omega, \tag{7}$$

where we have set

$$J(\mathbf{x}) = \det \mathbf{F}(\mathbf{x}), \quad \text{with} \quad \mathbf{F}(\mathbf{x}) = \mathbf{I} + \nabla \mathbf{u}(\mathbf{x}). \tag{8}$$

Forthcoming calculations involve expressing vectors and tensors in components. For this, we let $\{\mathbf{e}_1, \mathbf{e}_2, \mathbf{e}_3\}$ denote the canonical basis of the Euclidean space $\mathbb{R}^3$ and $\{x_1, x_2, x_3\}$ the associated coordinate system.

3.1 Energy of the Gel

As is customary in the gel literature, two different contributions to the total energy of a gel are considered. First, there is a contribution $\int_\Omega W_{el}(\mathbf{F}(\mathbf{x})) \, d\mathbf{x}$ associated to the elastic distortion of the polymer network. For simplicity, following Doi [14, Sects. 3.3.1, 3.3.2, 3.4.1], we assume that

$$W_{el}(\mathbf{F}) := \frac{G}{2} |\mathbf{F}|^2, \quad G > 0, \tag{9}$$

with an elastic modulus G that has dimensions of energy density. Second, we consider the Flory-Huggins energy of mixing ([14, Eq. 2.62], [29, p. 143]),

$$\int_{\Omega'} W_{FH}(\phi(\mathbf{y})) \, d\mathbf{y},$$

where

$$W_{FH}(\phi) := \frac{k_B T}{V_m} (\phi_1 \ln \phi_1 + \frac{1}{N} \phi_2 \ln \phi_2 + \chi \phi_1 \phi_2), \quad \phi_1 := 1 - \phi, \quad \phi_2 = \phi. \tag{10}$$

Here V_m represents the volume occupied by one solvent molecule; k_B is the Boltzmann constant; $N \gg 1$ is the number of segments of occupied by the polymer in the lattice model for polymer solutions (the solvent molecules being assumed to occupy each a single lattice site); and χ is the Flory-Huggins interaction parameter. The first and second terms in (10) correspond to the entropy of the fluid and polymer, respectively, and the third term represents attractive or repulsive interactions between two components.

The mixing energy density must be integrated on the current (swollen) configuration, where the interaction between the two species takes place. So as to be able to compare it against the elastic energy, we map it back to the original (Lagrangian) variables, obtaining

$$\int_\Omega W_{FH}(\phi(\mathbf{x} + \mathbf{u}(\mathbf{x}))) \det \mathbf{F}(\mathbf{x}) \, dx.$$

Let us introduce the notation

$$\nu := \frac{k_B T}{V_m}, \quad \gamma := \frac{G}{\nu}, \quad J := \det F,$$

and the dimensionless expression

$$H(J) := \frac{1}{\nu} J \, W_{\text{FH}}(\phi), \quad \phi = \phi_0/J,$$

$$= \frac{1}{N}\phi_0 \ln \frac{\phi_0}{J} + (J - \phi_0)\ln(1 - \frac{\phi_0}{J}) + \phi_0 \chi (1 - \frac{\phi_0}{J}), \quad J > 1. \tag{11}$$

We will take ν as a reference energy density unit. Dividing the total energy of the gel by ν and by its volume in the initial state, and taking the mass balance equation (7) into account, we arrive finally at the following dimensionless quantity:

$$E = \int_\Omega \frac{\gamma}{2}|\mathbf{F}|^2 + H(J)\,dx, \tag{12}$$

where $\int$ denotes the average integral.

In this article we will neglect the effect of gravity and of the external fluid pressure on the unbonded surfaces. Were they to be included, the corresponding additional terms would be: on the one hand, $\int \frac{\rho_0 g}{\nu}(x_2 + u_2(\mathbf{x}))\,d\mathbf{x}$, where ρ_0 is the density of gel in the reference configuration, g is the gravitational acceleration, and u_2 is the vertical displacement; on the other hand, $\int \frac{P_0}{\nu}J\,d\mathbf{x}$, assuming the external pressure to be constant and equal to P_0.

Determining the values of χ such that $H(J)$ is convex and finding the critical value χ_c above which the convexity is lost is relevant to our problem [14, Sect. 2.4]. In the later case, the gel separates into the polymer and fluid phases, which is outside the regime relevant to the applications that we consider. A direct calculation gives

$$\omega(J) := H'(J) = -\frac{1}{\nu}\Pi(\phi) = -\frac{\phi}{N} + \ln(1-\phi) + \phi + \chi\phi^2, \quad \phi = \phi_0/J, \tag{13}$$

where

$$\Pi(\phi) := -W_{\text{FH}}(\phi) + \phi \frac{dW_{\text{FH}}}{d\phi} + W_{\text{FH}}(0) \tag{14}$$

is the osmotic pressure of the polymer solution. Also,

$$H''(J) = \frac{\phi}{\nu J}\frac{d\Pi}{d\phi} = \frac{\phi}{J}\left(\frac{1}{N} + \frac{1}{1-\phi} - 1 - 2\chi\phi\right). \tag{15}$$

Hence $H(J)$ is convex in the whole range $J \in (\phi_0, \infty)$ if and only if [14, Eq. 2.67]

$$\chi < \underbrace{\frac{1}{2}\left(1 + \frac{1}{\sqrt{N}}\right)^2}_{:=\chi_c}. \tag{16}$$

This range for χ corresponds to the mixing regime for the gel [29]. Furthermore, since H is convex then the energy density $\frac{\gamma}{2}|\mathbf{F}|^2 + H(\det \mathbf{F})$ in (12) is a polyconvex function [3, 12] of the deformation gradient, and energy minimizers, under appropriate boundary conditions, are expected to exist [3, 12, 25].

From now on, we will consider the $N \to \infty$ approximation for the mixing energy of the gel. Hence, we will use the following expressions to determine, in Sect. 3.4, the Flory-Huggins interaction parameter χ and in the numerical simulations presented in Sect. 4:

$$H(J) = (J - \phi_0)\ln(1 - \phi) + \chi\phi_0(1 - \phi), \quad \phi = \phi_0/J, \tag{17}$$
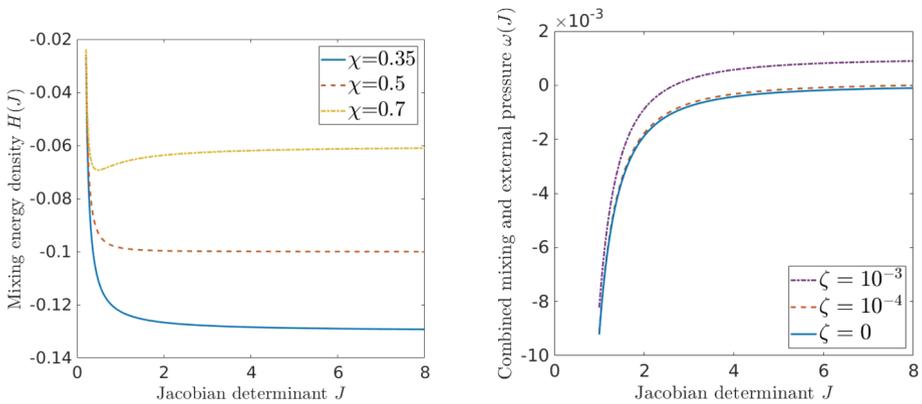
Fig. 3 Plots of $H(J)$ (left) and $\omega(J) := H'(J) + \zeta$, with $\zeta = P_0/\nu$ (right) as functions of the Jacobian determinant J. Note the loss of convexity of H as χ increases. In both graphs, we set $\phi_0 = 0.2$, as in (1). For the plot on the right we set $\chi = 0.348$, as in (31). The plot shows that the external fluid pressure can be neglected in the applications that we consider, since arterial pressures are normally of the order of 8–16 kPa, which makes the ratio $\zeta = P_0/\nu$ (of the external pressure to the reference energy density unit $\nu \approx 136.6$ MPa) of the order of $\zeta \sim 10^{-4}$

$$\omega(J) = H'(J) = -\frac{1}{\nu}\Pi(\phi) = \ln(1-\phi) + \phi + \chi\phi^2, \tag{18}$$

$$\chi_c = \frac{1}{2}. \tag{19}$$

3.2 Cauchy and Piola-Kirchhoff Stress Tensors

We now introduce the Piola-Kirchhoff stress tensor, which can be obtained by differentiating the (Lagrangian) energy density

$$W_{\text{el}}(\mathbf{F}) + W_{\text{FH}}(\phi_0/\det \mathbf{F})\det \mathbf{F}$$

with respect to the deformation gradient $\mathbf{F}$. Denoting the cofactor matrix of $\mathbf{F}$ by $\mathbf{F}^c$ we obtain

$$\mathbf{P} = G\mathbf{F} - \Pi(\phi)\mathbf{F}^c = \nu\left(\gamma\mathbf{F} + \omega(J)\mathbf{F}^c\right), \tag{20}$$

where we have used that the term $W_{\text{FH}}(0)$ in the definition of the osmotic pressure, given in (14), vanishes. (Recall the definition of $\omega(J)$ as $H'(J)$ in (13) and (18).) The corresponding Cauchy stress tensor is

$$\mathbf{T} = J^{-1}\mathbf{P}\mathbf{F}^T = GJ^{-1}\mathbf{F}\mathbf{F}^T - \Pi(\phi)\mathbf{I} = \nu\left(\gamma J^{-1}\mathbf{F}\mathbf{F}^T + \omega(J)\mathbf{I}\right). \tag{21}$$

From this expression for the Cauchy stress it is clear that the term $\nu\omega(J)F^c$ in the Piola-Kirchhoff stress is actually a pressure term associated to the change in volume. The tensor $\mathbf{P}$ consists of the elastic stress $G\mathbf{F} = \nu\gamma\mathbf{F}$ and the osmotic (Eulerian) pressure $-\Pi\mathbf{F}^c$ coming from the entropic Flory-Huggins energy. (In case the external fluid pressure were considered, the total Eulerian pressure to be equilibrated with the elastic stress would be $-\Pi + P_0 = \nu\omega(J)$, with $\omega(J) = H'(J) + P_0/\nu$.) In classical incompressible elasticity
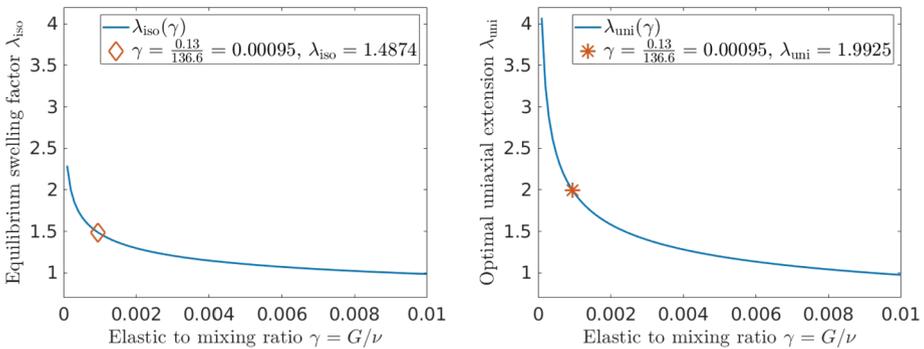
Fig. 4 The left and right plots represent λ_{iso} and λ_{uni}, respectively, for values of γ between 10^{-4} and 10^{-2}. (This corresponds to elastic moduli ranging from tens of kilopascals to a few megapascals.) The plots were made setting $\phi_0 = 0.2$ and $\chi = 0.348$

(without mixing), the Cauchy stress tensor is composed of a term coming from the derivatives of the stored-energy function $W_{\text{el}}(\mathbf{F})$ with respect to $\mathbf{F}$, and a pressure term that enforces the kinematic constraint of incompressibility. For example, when $W_{\text{el}}(\mathbf{F}) = \frac{G}{2}|\mathbf{F}|^2$, as in (9), then the Cauchy stress is given by $GJ^{-1}FF^T - p(\mathbf{x})\mathbf{I}$ for some Lagrange multiplier $p(\mathbf{x})$. Comparing it with (21), replacing p with the osmotic pressure Π, the same mathematical structure is found in the hydrogel model, even though the mechanics are very different (recall, in particular, that here the mixture is a new material that is not incompressible, even if its constituents are).

The traction boundary conditions due to the external pressure correspond to the balance of internal and external forces at the boundary, namely, the relation $P\mathbf{n}_0 = 0$, where $\mathbf{n}_0$ denotes the unit normal to $\partial\Omega$. Using (20), the condition can be formulated as

$$\omega(J)\mathbf{F}^c\mathbf{n}_0 = -\gamma\mathbf{F}\mathbf{n}_0. \tag{22}$$

3.3 Minimum Energy Solutions

As a consequence of the isotropy assumption on the gel, the stress-free states are isotropic expansions, that is, homogeneous solutions with a constant deformation gradient of the form

$$\mathbf{F} = \lambda_{\text{iso}}\mathbf{R}, \quad \mathbf{R} \in SO(3) \tag{23}$$

such that $\mathbf{P} = 0$ (see [14, Chap. 3], [10]). Taking $\mathbf{F}$ as in (23), from (20) we obtain

$$J_{\text{iso}}^{1/3}\omega(J_{\text{iso}}) = -\gamma, \quad J_{\text{iso}} := \lambda_{\text{iso}}^3, \tag{24}$$

or

$$\left(\phi_0/\phi^*\right)^{1/3}\omega\left(\phi_0/\phi^*\right) = -\gamma, \quad \text{with } \phi^* := \phi_0(\lambda_{\text{iso}})^{-3}. \tag{25}$$

The equilibrium swelling factor ϕ^*, depends on the initial polymer volume fraction ϕ_0 and the Flory-Huggins parameter, and has a prominent role in the study of gels [14, Chap. 3].

Other types of uniform solutions that will play a role in this paper are those with a uniaxial extension along the direction normal to the bonding substrate:

$$F = \text{diag}(1, \lambda_{\text{uni}}, 1), \tag{26}$$

with λ_{uni} given by the pressure boundary condition (22) along the vertical direction $\mathbf{n}_0 = \mathbf{e}_2$:

$$\omega(\lambda_{\text{uni}}) = -\gamma\lambda_{\text{uni}}. \tag{27}$$

The dependence of λ_{iso} and λ_{uni} on the (elastic vs. mixing) ratio γ is depicted in Fig. 4.

3.4 Determining the Flory-Huggins Parameter χ

According to Eqs. (18) and (24), in the free swelling experiment the gel is predicted to undergo an isotropic expansion whose determinant J_{iso} satisfies

$$\ln(1 - \phi^*) + \phi^* + \chi(\phi^*)^2 = -\gamma J_{\text{iso}}^{-1/3}, \quad \phi^* = \phi_0/J_{\text{iso}}. \tag{28}$$

Hence, χ can be retrieved from ϕ_0 and J_{iso} as:

$$\chi = -(\phi^*)^{-2}\left(\frac{G}{\nu}J_{\text{iso}}^{-1/3} + \ln(1 - \phi^*) + \phi^*\right), \quad \phi^* = \phi_0/J_{\text{iso}}, \quad \nu = \frac{k_B T}{V_m}. \tag{29}$$

Replacing J_{iso} with the experimental value of $J = 3.29$ reported in Sect. 2.3.1; ϕ_0 with the value $\phi_0 = 0.2$ reported in Sect. 2.2.1; G with the value $G = 0.13$ MPa in Sect. 2.3.3; the temperature with the value $T = 296$ K in Sect. 2.2.2, and V_m with the volume $V_m = 2.99151095 \cdot 10^{-29}$ m^3 of a single molecule of water, yields

$$\nu = 136.6 \text{ MPa} \tag{30}$$

and

$$\chi = 0.348 \tag{31}$$

as the Flory-Huggins interaction parameter χ (with three-digits precision[1]) for the PAAm gel.

3.5 Boundary Value Problem

3.5.1 Nondimensionalization

Let us denote the length, thickness, and width of the gel in its initial state by ℓ, d, and w. Placing the origin at the middle of the bottom surface of the rectangular gel, we obtain:

$$\Omega = \{(x_1, x_2, x_3): \quad -\frac{\ell}{2} < x_1 < \frac{\ell}{2}, \quad 0 < x_2 < d, \quad -\frac{w}{2} < x_3 < \frac{w}{2}\}. \tag{32}$$

We first scale the variables and fields of the problem according to the dimensions of the domain:

$$\xi_1 = \frac{x_1}{\ell}, \quad \xi_2 = \frac{x_2}{d}, \quad \xi_3 = \frac{x_3}{w}; \tag{33}$$

$$\upsilon_1(\boldsymbol{\xi}) = \frac{x_1 + u_1(\mathbf{x})}{\ell}, \quad \upsilon_2(\boldsymbol{\xi}) = \frac{x_2 + u_2(\mathbf{x})}{d}, \quad \upsilon_3(\boldsymbol{\xi}) = \frac{x_3 + u_3(\mathbf{x})}{w}. \tag{34}$$

---

[1]Rounding up χ to $\chi = 0.35$ already has an impact on the value of λ_{iso} in Eq. (24), turning it into $\lambda_{\text{iso}} = 1.48$ instead of the experimentally observed value of $\hat{\lambda}_{\text{iso}} = 1.49$.

The previous expressions render the deformation field $\boldsymbol{v}(\boldsymbol{\xi})$ dimensionless. Set

$$\eta := d/\ell, \quad \theta := w/\ell. \tag{35}$$

We aim to show that as η becomes increasingly smaller (while $\theta = w/\ell$ remains fixed), the solution to the boundary value problem corresponding to the completely bonded experiment becomes arbitrarily close to a uniform uniaxial extension by a factor of λ_{uni} in the direction normal to the substrate, where λ_{uni} is the value uniquely determined by Eq. (27). Using the chain rule we find the following expression for the deformation gradient and its determinant:

$$\mathbf{F} = \mathbf{I} + \nabla \mathbf{u}(\mathbf{x}) = \begin{pmatrix} \partial_1 v_1 & \eta^{-1}\partial_2 v_1 & \theta^{-1}\partial_3 v_1 \\ \eta\partial_1 v_2 & \partial_2 v_2 & \eta\theta^{-1}\partial_3 v_2 \\ \theta\partial_1 v_3 & \theta\eta^{-1}\partial_2 v_3 & \partial_3 v_3 \end{pmatrix} \tag{36}$$

$$J = \det \mathbf{F} = \det \left(\begin{pmatrix} \ell & & \\ & d & \\ & & w \end{pmatrix} \begin{pmatrix} \partial_1 v_1 & \partial_2 v_1 & \partial_3 v_1 \\ \partial_1 v_2 & \partial_2 v_2 & \partial_3 v_2 \\ \partial_1 v_3 & \partial_2 v_3 & \partial_3 v_3 \end{pmatrix} \begin{pmatrix} \ell^{-1} & & \\ & d^{-1} & \\ & & w^{-1} \end{pmatrix} \right) \tag{37}$$

$$= \frac{\partial(v_1, v_2, v_3)}{\partial(\xi_1, \xi_2, \xi_3)}.$$

The total energy per volume (12), in the reference energy density unit ν, becomes:

$$E = \int_{-1/2}^{1/2} \int_0^1 \int_{-1/2}^{1/2} \left(\frac{\gamma}{2}|\mathbf{F}|^2 + H(J) \right) \mathrm{d}\xi_3\,\mathrm{d}\xi_2\,\mathrm{d}\xi_1. \tag{38}$$

3.5.2 Governing Equations

The Euler-Lagrange equations for this energy functional are:

$$\gamma\frac{\partial^2 v_1}{\partial\xi_1^2} + \frac{\gamma}{\eta^2}\frac{\partial^2 v_1}{\partial\xi_2^2} + \frac{\gamma}{\theta^2}\frac{\partial^2 v_1}{\partial\xi_3^2} + \mathrm{div}_{\boldsymbol{\xi}}\left(\omega(J)\Big(\frac{\partial(v_2, v_3)}{\partial(\xi_2, \xi_3)}, \frac{\partial(v_2, v_3)}{\partial(\xi_3, \xi_1)}, \frac{\partial(v_2, v_3)}{\partial(\xi_1, \xi_2)}\Big) \right) = 0 \tag{39}$$

$$\eta^2\gamma\frac{\partial^2 v_2}{\partial\xi_1^2} + \gamma\frac{\partial^2 v_2}{\partial\xi_2^2} + \eta^2\frac{\gamma}{\theta^2}\frac{\partial^2 v_2}{\partial\xi_3^2} + \mathrm{div}_{\boldsymbol{\xi}}\left(\omega(J)\Big(\frac{\partial(v_3, v_1)}{\partial(\xi_2, \xi_3)}, \frac{\partial(v_3, v_1)}{\partial(\xi_3, \xi_1)}, \frac{\partial(v_3, v_1)}{\partial(\xi_1, \xi_2)}\Big) \right) = 0 \tag{40}$$

$$\theta^2\gamma\frac{\partial^2 v_3}{\partial\xi_1^2} + \theta^2\frac{\gamma}{\eta^2}\frac{\partial^2 v_3}{\partial\xi_2^2} + \gamma\frac{\partial^2 v_3}{\partial\xi_3^2} + \mathrm{div}_{\boldsymbol{\xi}}\left(\omega(J)\Big(\frac{\partial(v_1, v_2)}{\partial(\xi_2, \xi_3)}, \frac{\partial(v_1, v_2)}{\partial(\xi_3, \xi_1)}, \frac{\partial(v_1, v_2)}{\partial(\xi_1, \xi_2)}\Big) \right) = 0. \tag{41}$$

Thanks to Piola's identity [11], by which the cofactor matrix of $\nabla_{\boldsymbol{\xi}}\boldsymbol{v}$ is divergence-free, the equations can be rewritten as

$$\gamma\frac{\partial^2 v_1}{\partial\xi_1^2} + \frac{\gamma}{\eta^2}\frac{\partial^2 v_1}{\partial\xi_2^2} + \frac{\gamma}{\theta^2}\frac{\partial^2 v_1}{\partial\xi_3^2} + H''(J)\frac{\partial(J, v_2, v_3)}{\partial(\xi_1, \xi_2, \xi_3)} = 0 \tag{42}$$

$$\eta^2\gamma\frac{\partial^2 v_2}{\partial\xi_1^2} + \gamma\frac{\partial^2 v_2}{\partial\xi_2^2} + \eta^2\frac{\gamma}{\theta^2}\frac{\partial^2 v_2}{\partial\xi_3^2} + H''(J)\frac{\partial(v_1, J, v_3)}{\partial(\xi_1, \xi_2, \xi_3)} = 0 \tag{43}$$

$$\theta^2 \gamma \frac{\partial^2 \upsilon_3}{\partial \xi_1^2} + \theta^2 \frac{\gamma}{\eta^2} \frac{\partial^2 \upsilon_3}{\partial \xi_2^2} + \gamma \frac{\partial^2 \upsilon_3}{\partial \xi_3^2} + H''(J) \frac{\partial(\upsilon_1, \upsilon_2, J)}{\partial(\xi_1, \xi_2, \xi_3)} = 0. \tag{44}$$

3.5.3 Boundary Conditions

Free swelling experiment. For the free swelling experiment we impose the zero traction boundary condition (22) on all the six faces of the rectangular gel. It can be verified easily that the deformation map

$$x_1 + u_1(\mathbf{x}) = \lambda_{\mathrm{iso}} x_1, \quad x_2 + u_2(\mathbf{x}) = \lambda_{\mathrm{iso}} x_2, \quad x_3 + u_3(\mathbf{x}) = \lambda_{\mathrm{iso}} x_3, \tag{45}$$

with λ_{iso} given by (24), which corresponds to $\boldsymbol{\upsilon}(\boldsymbol{\xi}) = \lambda_{\mathrm{iso}} \boldsymbol{\xi}$, solves the boundary value problem. The same can be said if the isotropic expansion (45) is followed, or preceded, by a rotation and/or a translation. Presumably, these constitute all the minimizers of the energy of the gel.

Completely bonded gel. For the case of a gel bonded to a glass slide on the bottom surface, we will assume that the bonding is infinitely strong so that a zero displacement boundary condition can be imposed at the gel/substrate interface:

$$\boldsymbol{\upsilon}(\xi_1, 0, \xi_3) = (\xi_1, 0, \xi_3), \quad -\frac{1}{2} < \xi_1, \xi_3 < \frac{1}{2}. \tag{46}$$

At the remaining five faces of the rectangular gel we impose the zero traction boundary condition (22). On the top surface it reads

$$\begin{aligned}
\omega(J)\eta \frac{\partial(\upsilon_2, \upsilon_3)}{\partial(\xi_3, \xi_1)} &= -\gamma \eta^{-1} \partial_2 \upsilon_1, \\
\omega(J) \frac{\partial(\upsilon_3, \upsilon_1)}{\partial(\xi_3, \xi_1)} &= -\gamma \partial_2 \upsilon_2, \quad \omega(J)\eta \frac{\partial(\upsilon_1, \upsilon_2)}{\partial(\xi_3, \xi_1)} = -\gamma \theta \eta^{-1} \partial_2 \upsilon_3.
\end{aligned} \tag{47}$$

At the left and the right surfaces, the traction-free condition is

$$\begin{aligned}
\omega(J) \frac{\partial(\upsilon_2, \upsilon_3)}{\partial(\xi_2, \xi_3)} &= -\gamma \partial_1 \upsilon_1, \\
\omega(J)\eta^{-1} \frac{\partial(\upsilon_3, \upsilon_1)}{\partial(\xi_2, \xi_3)} &= -\gamma \eta \partial_1 \upsilon_2, \quad \omega(J)\theta^{-1} \frac{\partial(\upsilon_1, \upsilon_2)}{\partial(\xi_2, \xi_3)} = -\gamma \theta \partial_1 \upsilon_3.
\end{aligned} \tag{48}$$

At the front and at the back of the gel, the condition is

$$\begin{aligned}
\omega(J)\theta \frac{\partial(\upsilon_2, \upsilon_3)}{\partial(\xi_1, \xi_2)} &= -\gamma \theta^{-1} \partial_3 \upsilon_1, \\
\omega(J)\theta \eta^{-1} \frac{\partial(\upsilon_3, \upsilon_1)}{\partial(\xi_1, \xi_2)} &= -\gamma \eta \theta^{-1} \partial_3 \upsilon_2, \quad \omega(J) \frac{\partial(\upsilon_1, \upsilon_2)}{\partial(\xi_1, \xi_2)} = -\gamma \partial_3 \upsilon_3.
\end{aligned} \tag{49}$$

3.6 Thin Film Limit

Imagine a sequence $\left(\Omega^{(j)}\right)_{j \in \mathbb{N}}$ of ever thinner rectangular prisms with dimensions $\ell^{(j)}$, $d^{(j)}$, $w^{(j)}$, such that the ratio $w^{(j)}/\ell^{(j)}$ of their widths and lengths remains constant and the ratio $d^{(j)}/\ell^{(j)}$ tends to zero as $j \to \infty$:

$$\eta^{(j)} = \frac{d^{(j)}}{\ell^{(j)}} \xrightarrow{j \to \infty} 0, \quad \frac{w^{(j)}}{\ell^{(j)}} = \theta \quad \text{for all } j \in \mathbb{N}. \tag{50}$$

For each fixed j, the total (nondimensionalized) energy E in (38), which we will now denote by $E^{(j)}$, depends on j through the term $|\mathbf{F}|^2$; specifically, through the parameter η appearing in (36). Suppose that we can find a sequence $\left(\boldsymbol{v}^{(j)}\right)_{j \in \mathbb{N}}$ of maps from the (fixed) unit cube $(-1/2, 1/2) \times (0, 1) \times (-1/2, 1/2)$ to $\mathbb{R}^3$, each of them fulfilling the zero-displacement condition (46) at the bottom surface, such that for each $j \in \mathbb{N}$ the function $\boldsymbol{v}^{(j)}$ minimizes the energy $E^{(j)}$ in a suitable admissible class of orientation-preserving and injective maps from the unit cube to $\mathbb{R}^3$ satisfying the bonding condition (46). In particular, we shall assume that, for each j, $\boldsymbol{v}^{(j)}$ solves the governing partial differential equations and corresponding zero-traction conditions. Now assume that, furthermore, the maps $\boldsymbol{v}^{(j)}$ converge, in a suitable sense, to some limit map (v_1, v_2, v_3). We will study the limit equations satisfied by $\boldsymbol{v}$.

First of all, the explosive terms with a prefactor η^{-2} in Eqs. (42)–(44) can be assumed (formally) to vanish in the thin film $\eta^{(j)} \to 0$ limit (since none of the remaining terms blow up and are, thus, unable to equilibrate them). Therefore,

$$\frac{\partial^2 v_1}{\partial \xi_2^2} \equiv \frac{\partial^2 v_3}{\partial \xi_2^2} \equiv 0. \tag{51}$$

Consequently, the dependence on the vertical coordinate ξ_2 is affine (with coefficients depending on ξ_1, ξ_3) both for v_1 and v_3.

The traction condition (47) on the top surface suggests that both $\partial_2 v_1^{(j)}$ and $\partial_2 v_3^{(j)}$ are of order $\left(\eta^{(j)}\right)^2$. Hence, in the limit, both $\partial_2 v_1$ and $\partial_2 v_3$ vanish at $\xi_2 = 1$. Since, for every fixed (ξ_1, ξ_3) at the basis, the derivatives $\partial_2 v_1$ and $\partial_2 v_3$ are independent of ξ_2, it follows that

$$\text{for all } (\xi_1, \xi_2, \xi_3), \quad \partial_2 v_i(\xi_1, \xi_2, \xi_3) = \partial_2 v_i(\xi_1, 1, \xi_3) = 0. \tag{52}$$

This implies that v_1 and v_3 themselves (not only their vertical derivatives) are independent of ξ_2. Combining this with the bonding condition at the bottom, we obtain

$$v_1(\xi_1, \xi_2, \xi_3) = \xi_1, \quad v_3(\xi_1, \xi_2, \xi_3) = \xi_3 \quad \text{for all } (\xi_1, \xi_2, \xi_3). \tag{53}$$

Plugging the above into the expression (36) for the deformation gradient yields

$$\mathbf{F} = \begin{pmatrix} 1 & 0 & 0 \\ 0 \cdot \partial_1 v_2 & \partial_2 v_2 & 0 \cdot \theta^{-1} \cdot \partial_3 v_2 \\ 0 & 0 & 1 \end{pmatrix} = \begin{pmatrix} 1 & & \\ & \partial_2 v_2 & \\ & & 1 \end{pmatrix}. \tag{54}$$

One of the consequences is that

$$J(\xi_1, \xi_2, \xi_3) = \det \mathbf{F} = \partial_2 v_2(\xi_1, \xi_2, \xi_3). \tag{55}$$

Let us call $\beta(\boldsymbol{\xi})$ to

$$\beta(\boldsymbol{\xi}) := \frac{\partial v_2}{\partial \xi_2}(\boldsymbol{\xi}), \quad \boldsymbol{\xi} \in (-1/2, 1/2) \times (0, 1) \times (-1/2, 1/2). \tag{56}$$

With the previous findings, the equations (42)–(44) simplify to

$$H''(\beta(\boldsymbol{\xi})) \frac{\partial(\beta, v_2)}{\partial(\xi_1, \xi_2)} = 0, \tag{57}$$

$$\gamma \frac{\partial \beta}{\partial \xi_2} + H''(\beta(\boldsymbol{\xi})) \frac{\partial \beta}{\partial \xi_2} = 0, \tag{58}$$

$$H''\big(\beta(\boldsymbol{\xi})\big)\frac{\partial(\upsilon_2,\beta)}{\partial(\xi_2,\xi_3)}=0. \tag{59}$$

From Eq. (58), since we are in the mixing regime (16) for the gel in which $H''(J) > 0$ for all $J > \phi_0$, we conclude that the vertical stretch $\beta = \partial_2\upsilon_2$ is independent of ξ_2. On the other hand, the traction-free condition on the top surface shows that

$$\omega\big(\beta(\xi_1,1,\xi_3)\big)=-\gamma\beta(\xi_1,1,\xi_3). \tag{60}$$

Hence, for all $-\frac{1}{2} < \xi_1, \xi_3 < \frac{1}{2}$, the value of $\beta(\xi_1,1,\xi_3)$ is the unique solution[2] λ to the equation $\omega(\lambda) = -\gamma\lambda$, which is nothing other than the vertical stretch λ_{uni} in the energy-minimizing uniaxial extension of Sect. 3.3. Now, the bonding boundary condition at $\xi_2 = 0$ tells us that $\upsilon_2 \equiv 0$ on the gel/substrate interface. The fundamental theorem of calculus then gives us that

$$\text{for all } \xi_1,\xi_2,\xi_3: \quad \upsilon_2(\xi_1,\xi_2,\xi_3)=0+\int_0^{\xi_2}\partial_2\upsilon_2(\xi_1,s,\xi_3)\,\mathrm{d}s=\lambda_{\text{uni}}\xi_2. \tag{61}$$

All in all, together with (53), there is enough analytical evidence to conclude, at least formally, that the energy minimizers $\boldsymbol{\upsilon}^{(j)}$ converge, as $j \to \infty$, to a homogeneous uniaxial extension in the vertical direction, with principal stretches 1, λ_{uni}, and 1.

3.7 Comparison Between the Thin-Film-Limit Uniaxial Solution and the Vertical Stretches in the Completely Bonded Experiment

As mentioned in Sect. 2.3.2, the deformation observed in the completely bonded gel is indeed close to a homogeneous uniaxial extension. On the other hand, the perfectly uniaxial and uniform swelling is only achieved in the theoretical thin film limit. In a real sample, the aspect ratio η is small but not zero. The gel does take advantage of the liberty to swell outwards as one moves away from the confining glass slide. We already observed that the lateral displacement was between 1.85 and 2.0 mm towards the front, back, left, and right of the sample, which is a small displacement compared to the width of 15 mm in the reference configuration, and, most of all, compared to its length of 90 mm. Now we focus on the comparison between the theoretical prediction, in the idealized thin film limit, for the stretch in the vertical direction and the experimental observation.

First, for convenience, we have summarized the parameters of the model in Table 3. Plugging them into (27) and (18), using a nonlinear solver we obtain the theoretical value of

$$\lambda_{\text{uni}} = 1.99, \tag{62}$$

with two digits of precision. As mentioned in Sect. 2.3.2, the thickness of the swollen gel, measured in the middle region, was approximately 3.40 mm. This corresponds to a vertical extension by a factor of

$$\hat{\lambda}_{\text{uni}} = 3.40/1.62 \approx 2.10, \tag{63}$$

since the thickness before immersing the PAAm gel into water was of 1.62 mm. The experimental and theoretical values $\hat{\lambda}_{\text{uni}}$ and λ_{uni} differed, therefore, by 5% (relative to each other).

---

[2]It can be seen that the solution is unique because $\omega(J)$ is an increasing function of J, since we are in the mixing regime where $\omega'(J) = H''(J) > 0$ for all $J > \phi_0$.

Table 3 Parameters of the model and their symbols

Reference polymer volume fraction	ϕ_0	0.2
Elastic shear modulus	G	0.13 MPa
Flory-Huggins parameter	χ	0.348
Absolute temperature	T	296 K
Boltzmann constant	k_B	$1.38064852 * 10^{-23} \ \mathrm{m^2 \ kg \ s^{-2} \ K^{-1}}$
Volume of a water molecule	V_m	$3 * 10^{-29} \ \mathrm{m^3}$
Energy per unit volume	$\nu = \frac{K_B T}{V_m}$	136.6 MPa
Elastic vs. mixing energy density ratio	$\gamma = \frac{G}{\nu}$	0.00095

3.8 Formula for the Threshold Thickness in a Simplified 2D Setting

Consider, in this subsection only, the simplified situation in which the gel is placed between two parallel walls at the front and at the back (that is, following the notation of (32), walls along the planes $x_3 = \frac{w}{2}$ and $x_3 = -\frac{w}{2}$, respectively), along which it is free to slide. The gel can only swell in the direction normal to the substrate and along the length direction, so that the nondimensionalized deformation map $\boldsymbol{\xi} = \left(\frac{x_1}{\ell}, \frac{x_2}{d}, \frac{x_3}{w} \right) \in \Omega \mapsto (\upsilon_1, \upsilon_2, \upsilon_3)$ of Eq. (34) takes the form

$$\upsilon_1(\boldsymbol{\xi}) = \frac{x_1 + u_1(x_1, x_2)}{\ell}, \quad \upsilon_2(\boldsymbol{\xi}) = \frac{x_2 + u_2(x_1, x_2)}{d}, \quad u_3(\mathbf{x}) = 0. \tag{64}$$

The expression for the deformation gradient simplifies to

$$\mathbf{F} = \mathbf{I} + \nabla \mathbf{u}(\mathbf{x}) = \begin{pmatrix} \partial_1 \upsilon_1 & \eta^{-1} \partial_2 \upsilon_1 & 0 \\ \eta \partial_1 \upsilon_2 & \partial_2 \upsilon_2 & 0 \\ 0 & 0 & 1 \end{pmatrix}. \tag{65}$$

With this simpler expression, it is possible to study the stability of the gel against debonding, following the principle in fracture mechanics [1, 7, 17, 18] that if the free energy released by the detachment of the gel, at a certain portion of the bonding interface, is insufficient to compensate the energy required for detachment, then the breaking of bonds will not be observed. Assuming that the debonding is produced at the left and right ends of the interface with the substrate, and that the solution is symmetric with respect to the vertical plane $\{x_1 = 0\}$, we are left to study the minimization of the free energy

$$|\Omega| \cdot E = \ell d w \nu \int_{-1/2}^{1/2} \int_0^1 \int_{-1/2}^{1/2} \left(\frac{\gamma}{2} |\mathbf{F}|^2 + H(\det \mathbf{F}) \right) d\xi_3 \, d\xi_2 \, d\xi_1$$

$$= 2\ell d w \nu \int_0^{1/2} \int_0^1 \frac{\gamma}{2} \left((\partial_1 \upsilon_1)^2 + \eta^{-2}(\partial_2 \upsilon_1) + \eta^2 (\partial_1 \upsilon_2)^2 + (\partial_2 \upsilon_2)^2 + 1 \right)$$

$$+ H\left(\begin{vmatrix} \partial_1 \upsilon_1 & \partial_2 \upsilon_1 \\ \partial_1 \upsilon_2 & \partial_2 \upsilon_2 \end{vmatrix} \right) d\xi_2 \, d\xi_1$$

among all admissible deformations satisfying the zero displacement boundary condition only at a fraction δ of the interface:

$$v_1(\xi_1, 0, \xi_3) = \xi_1 \quad \text{and} \quad v_2(\xi_1, 0, \xi_3) = 0 \quad \text{for all} \quad -\frac{\delta}{2} < \xi_1 < \frac{\delta}{2},$$

where $0 < \delta < 1$ is the proportion of the interface that remains bonded and E is the energy per unit volume (38) measured taking $v = \frac{k_B T}{V_m}$ as the reference energy density unit. Let us denote, for every fixed $0 < \delta < 1$, the minimum energy by $E_{\min}[\delta]$. Then, the rate of change (per unit increase in debonded area) is to be compared against the adhesive toughness σ (the fracture energy required per unit debonded area):

$$\frac{\left| \frac{\mathrm{d}}{\mathrm{d}\delta} \left(\ell d w v \cdot E_{\min}[\delta] \right) \right|}{\left| \frac{\mathrm{d}}{\mathrm{d}\delta} \left((1 - \delta)\ell w \right) \right|} \le \sigma.$$

This yields the following threshold for the thickness of the gel below which it can be expected to be stable against debonding:

$$d \le d_{\max} := \frac{\sigma}{v R(\chi, G, \phi_0)}, \quad R(\chi, G, \phi_0) := \frac{\mathrm{d}}{\mathrm{d}\delta} E_{\min}[\delta].$$

As argued in [9], a formal asymptotic analysis indicates that as the aspect ratio $\eta = d/\ell$ vanishes any sequence of solutions to the equilibrium equations converges pointwise to the piecewise affine deformation

$$(v_1, v_2) = \begin{cases} (\xi_1, \ \lambda_{\mathrm{uni}}\xi_2), & \text{if } \xi_1 \le \delta \\ \left(\lambda^*\xi_1 + \delta(1 - \lambda^*), \ \lambda^*\xi_2 + \beta_0 \right), & \text{if } \delta \le \xi_1 \le 1 \end{cases},$$

for a certain constant $\beta_0 > 0$, where λ_{uni} is the optimal stretch factor (27) for a uniaxial swelling normal to the substrate and λ^* is the unique solution to

$$\omega\left((\lambda^*)^2 \right) = -\gamma, \tag{66}$$

which corresponds to the optimal stretch factor for a equi-biaxial swelling along the vertical and the length directions. Therefore, to first order the threshold thickness is given by

$$d_{\max} = \frac{\sigma}{v \left(\left(\frac{\gamma}{2}(2 + \lambda_{\mathrm{uni}}^2) + H(\lambda_{\mathrm{uni}}) \right) - \left(\frac{\gamma}{2}(2(\lambda^*)^2 + 1) + H\left((\lambda^*)^2 \right) \right) \right)},$$

that is,

$$d_{\max} = \frac{\sigma}{\frac{G}{2} \left(1 + \lambda_{\mathrm{uni}}^2 - 2(\lambda^*)^2 \right) + \frac{k_B T}{V_m} \left(H(\lambda_{\mathrm{uni}}) - H\left((\lambda^*)^2 \right) \right)}. \tag{67}$$

For example, taking $\phi_0 = 0.2$, $v = \frac{k_B T}{V_m} = 136.6$ MPa, $G = 0.13$ MPa, and $\chi = 0.348$, as in Sect. 3.4; for an adhesive toughness σ in the range from 1 to 2 kJ/ m^2 (see, e.g., [36]), the threshold thickness for stability obtained from the two-dimensional formula (67) goes from 9.6 to 19.3 mm.

We have thus shown that the formula obtained in [9, Eqs. (84)–(85)], taking a dry polymer as the reference configuration, remains unchanged in the real situation where the hydrogel in synthesis already contains a large amount of solvent (as reported in Sect. 2.2.1, the fluid phase occupies 80% of the initial volume in the PAAm gels synthetized in our experiments). The only difference for the value of the threshold thickness $d_{\max}$ between the model assuming a dry reference configuration and the more realistic model hereby considered comes from the dependence of $H(J)$, defined in (17), and the dependence of λ_{uni} and λ^*, through Eqs. (18), (27), and (66), on the initial polymer volume fraction ϕ_0.

4 Finite Element Simulations

Numerical simulations for both the free swelling and the completely bonded gels exposed to solvent were carried out. The free swelling situation served for validation purposes while the completely bonded simulation allowed for a comparison between the prediction of the model (without having to take the thin film limit) and the observations in the laboratory.

4.1 Methods

Simulations were carried out with the same values of the parameters as in Sect. 3.4

$$\phi_0 = 0.2, \quad \gamma = \frac{0.13}{136.6}, \quad \chi = 0.348. \tag{68}$$

For the finite element simulations, we discretize the computational domain with tetrahedral meshes and use continuous piecewise cubic finite element spaces to approximate the displacement variable. All the simulations were implemented in the open-source finite element library Netgen/NGSolve (www.ngsolve.org) [30]. The system of nonlinear equations arising from the finite element approximation of our nonlinear boundary value problems were solved using the damped Newton's method. However, the implementation of the Newton's method did not work well when the tangent stiffness was computed at states of large deformation (possibly because of the almost horizontal nature of the function $\omega(J)$ for large values of J, as can be seen in Fig. 3). This was particularly delicate in the case of the bonded gel experiment. To solve this problem, we propose a technique of 'incremental softening', solving the nonlinear system first for gels that are much more rigid (for values of γ five or ten times larger than the desired $\gamma = 0.13/136.6 \approx 10^{-3}$), and then using the previous solution as the first iteration of the Newton's method for the next (smaller) value of γ. The stopping criteria used was defined to be the following: that the absolute value of the L^2-inner product between the residuals and the difference of the successive solutions had to be less than a certain tolerance (or that a certain prescribed maximum number `maxits` of iterations were reached). The deformed configurations and color maps associated to the components of the displacement were finally visualized in ParaView. Note that mesh refinement at the corners of the sample did not give any noticeable difference in the solutions and, hence, for this problem, appears to be unnecessary.

4.1.1 Free Swelling

Solutions were sought among displacement fields that were symmetric with respect to the coordinate axes (placing the origin at the middle of the sample, also in the vertical direction). This was done in order to break the translational and rotational symmetry of the boundary
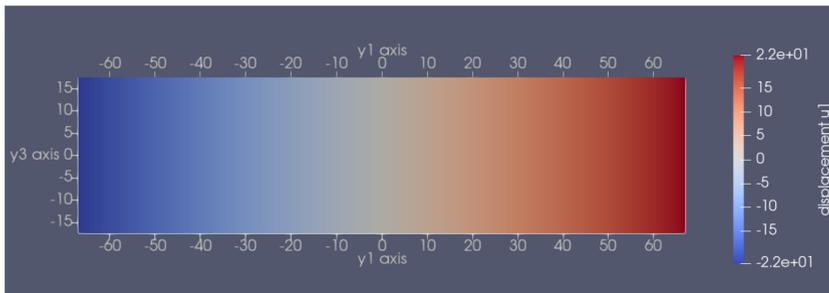
Fig. 5 Displacement towards the left and right (y_1 direction) as a colormap for the top view of the deformed gel in the free swelling experiment

value problem, thus falling into a problem with a unique solution. To implement this, the considered computational domain was only an octant of the rectangular prism representing the gel, and the slip boundary conditions $\mathbf{u}(\mathbf{x}) \cdot \mathbf{n}(\mathbf{x}) = 0$ were imposed for $\mathbf{x}$ on the three facets of the computational domain that belonged to the interior of the gel (one on the plane $x_1 = 0$, another on the plane $x_2 = 0$, and the remaining one on the plane $x_3 = 0$). The chosen length, thickness, and width (in mm) of the computational domain were, accordingly, half those reported in Sect. 2.2.2, namely: 45.0, 1.5, and 11.75, respectively. The specified parameter for the mesh generator prescribed that all elements in the triangulation had a diameter of less than 2 mm (interpreting the dimensions 45, 1.5, 11.75 of the computational domain as measured in mm). The damping parameter for the Newton's method was set to 0.1, the tolerance for the stopping criteria was 10^{-8} and `maxits` was 500.

4.1.2 Bonded Experiment

Length, thickness, and width (in mm) of the computational domain were chosen as those of the reference configuration in Sect. 2.2.3: 90.0, 1.62, and 15.0, respectively. Zero-displacement boundary conditions, $\mathbf{u}(\mathbf{x}) = \mathbf{0}$ for $\mathbf{x} = (x_1, 0, x_3)$, were imposed on the bottom surface. The specified parameter for the mesh generator prescribed that all elements in the triangulation had a diameter of less than 1 mm (interpreting the dimensions 90, 1.62, and 15 of the computational domain as measured in mm). The damping parameter for the Newton's method was set to be 0.05. In the process of 'incremental softening', 15 different values of γ were considered between 0.066 and the desired value of $0.13/136.6 \approx 0.00095$. In each of these 15 preparatory resolutions of the Newton's method, the chosen tolerance for the stopping criteria was 10^{-3} and `maxits=` 100. In the final resolution of the Newton's method, finally with the right value of γ, the chosen tolerance for the stopping criteria was 10^{-8} and `maxits` was 500.

4.2 Results

4.2.1 Free Swelling

Towards the left and the right of the sample (y_1 direction) the observed displacement is of 21.93 mm on each side (see Fig. 5). This corresponds to an extension by a factor of 1.49 along the length direction.

The upward and downward displacement, respectively, at the top and bottom surfaces, is of 0.73 mm. This is an extension by a factor of 1.49 in the vertical direction.
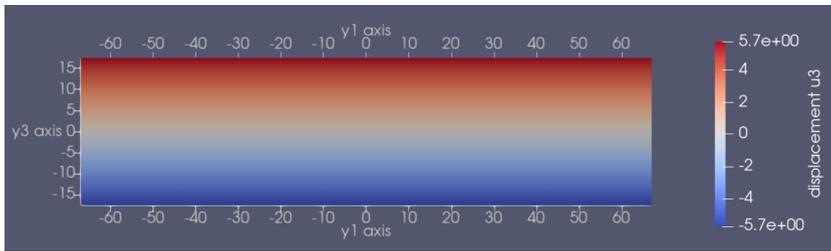
Fig. 6 Displacement towards the front and the back (y_3 direction) as a colormap for the top view of the deformed gel in the free swelling experiment
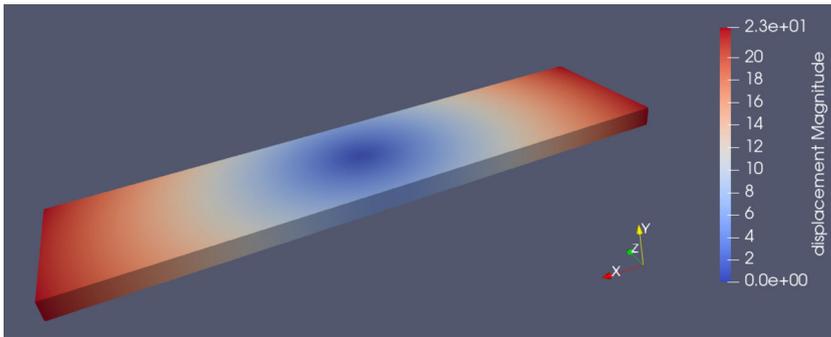
Fig. 7 Swollen configuration, with the magnitude of the displacement of each material point as the associated colormap. The colors indicate that the origin remains fixed and that the amount of displacement is proportional to the distance to the origin, which is characteristic of the isotropic expansion

Towards the front and the back of the sample (y_3 direction), the observed displacement is of 5.73 mm on each side (see Fig. 6). This corresponds to an extension by a factor of 1.49 along the width. All in all, the expected solution of an isotropic expansion with an strech of 1.49 is obtained in the numerical experiments (see Fig. 7), thus validating the correctness of the code and the accuracy of the approximation obtained with the fine meshes used.

4.2.2 Bonded Experiment

The obstacle problem: the first finite element simulations we performed for the gel completely bonded at its bottom surface showed that it is necessary to take into account that the glass slide in the experiment at the laboratory is larger than the base of the gel sample. The reason is that if nothing else is implemented apart from the zero-displacement boundary condition at the $\{x_2 = 0\}$ surface and the zero-traction natural boundary condition on the lateral and top surfaces of the domain, then a portion of the gel exhibits a downwards displacement that goes beyond the substrate level $y_2 = 0$ (even up to $y_2 = -0.32$ mm, which is significant compared to the initial thickness of 1.6 mm and the final thickness of 3.2 mm; see Fig. 8). Although this is observed only in a very small portion of the gel around the four bottom corners (inside the region $\{45.0 < |y_1| < 45.9, 6.5 < |y_3| < 8.5\}$), the formation of this bulge is counter intuitive. Since the bottom surface is subject to a zero-displacement boundary condition, the material points reaching deformed locations below the horizontal $y_2 = 0$ plane come from the lateral boundaries ($x_1 = \pm\ell/2$,
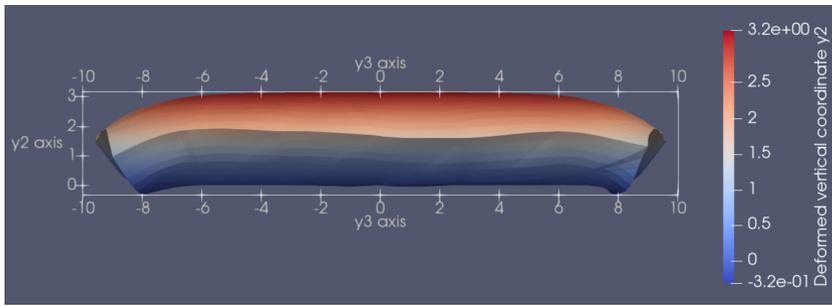
Fig. 8 Left view (slice at $x_1 = -45$) of the swollen specimen in the simulation without implementing the obstacle problem. The color map is associated to the vertical coordinate $y_2(\mathbf{x}) = x_2 + u_2(\mathbf{x})$ of the deformed material point, with extreme values of -0.32 and 3.17

$\ell = 90$, and $x_3 = \pm w/2$, $w = 15$) and from the interior of the gel. After a number of revisions, we are confident that it is an outcome of the model and not a numerical error. In particular, the gel still bulges from the lower corners even if the mesh is further refined at the corners. Presumably, it is the result of the need to compatibilize, on the one hand, the desire of the lateral faces to rotate in order to attain a multiaxial extension, and, on the one hand, the zero-displacement condition at the bottom surface.

In order to overcome this difficulty, we included a local repulsive force in the form of a penalty term added to the energy functional, so that minimizers were sought for

$$\int_\Omega \frac{\gamma}{2} |\mathbf{I} + \nabla \mathbf{u}|^2 + H(\det \nabla \mathbf{u}) + A \left| \left(x_2 + u_2(\mathbf{x}) \right)^- \right|^2 d\mathbf{x}, \quad A = 100000, \tag{69}$$

where the expression $(s)^-$ above denotes the negative part of s:

$$(s)^- = \begin{cases} |s|, & \text{if } s \le 0, \\ 0, & \text{if } s \ge 0. \end{cases}$$

If the penalty factor A were sent to infinity, minimizers for the penalized functional are expected to converge to minimizers of the original energy functional among deformations satisfying the Signorini constraint $y_2(\mathbf{x}) \ge 0$ for all $\mathbf{x} \in \Omega$ (which, in turn, satisfy the associated natural boundary conditions involving a normal reaction term in the parts of the boundary in contact with the substrate $\{y_2 = 0\}$). With the value chosen of $A = 100000$, the constraint $y_2 \ge 0$ is essentially fulfilled: for the detailed verification of this, the reader is referred to the Appendix.

Comparison with experiments: the deformed configuration at equilibrium is presented in Fig. 9. Most of the gel swells uniformly upwards, but a tendency lo lateral swelling is observed, and is more pronounced as one departs from the substrate, in agreement with the experimental observation.

The maximum vertical displacement, which is attained in almost all of the top surface, is 1.57 mm. This corresponds to a vertical stretch of 1.97, which captures the measurement in the laboratory of $\hat{\lambda}_{\text{uni}} = 2.10$ (see Sect. 3.7) with an error of 6.6%. The obtained vertical extension differs from the idealized thin-film-limit uniaxial extension of $\lambda_{\text{uni}} = 1.99$ by an error of 1%.
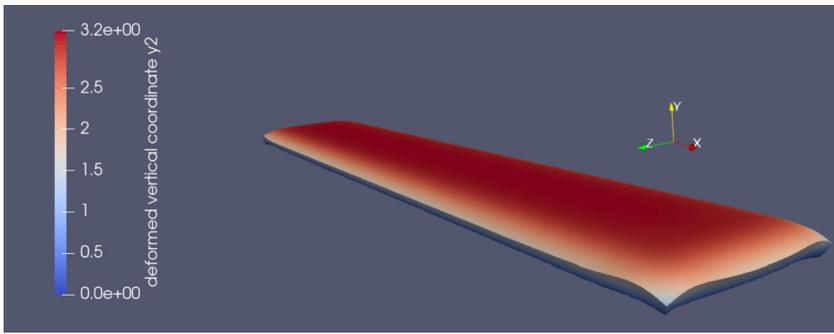
Fig. 9 Gel at numerical swelling equilibrium

The width of the swollen gel in the numerical simulation (in the y_3 direction) is of 19.12 mm, that is, 4.12 mm more than the 15 mm width in the reference state. This captures the measurement of 3.95 mm for the lateral swelling, obtained from f) in Sect. 2.3.2, by an error of 4.3%. Note that this larger lateral swelling, towards the front and the back, compensates the smaller vertical extension compared to the experiments.

The swollen gel is 93.98 mm long (in the y_1 direction) in the numerical simulation, capturing measurement d) of 93.73 mm in Sect. 2.3.2 by an error (3.98/3.73) of 6.7%.

Regarding why the swelling is comparable (of about 2.0 mm to each side) in the two horizontal directions y_1 and y_3, given that one of the dimensions (90 mm) is much larger than the other (15 mm), note that most of the swelling comes from a small portion near the lateral faces: points with a displacement of more than 0.5 mm towards the right are found only in $\{\mathbf{x} \in \Omega : 42.5 < x_1 \le 45\}$, and points with a displacement of more than 0.5 mm towards the front only in $\{\mathbf{x} \in \Omega : 4.2 < x_3 \le 7\}$.

Incorporating the effect of the interfacial energy between the polymer and the solvent might bring more accuracy in the model and will be part of future work.

5 Conclusions

This work emphasizes the connection between theory and experiments on the problems of swelling equilibria of free as well as fully bonded gels. We obtain a thin film limit of a three dimensional gel, without any intermediate two dimensional assumptions. We also outline a method to calculate experimental parameters by combining the theory with the laboratory measurements. Numerical simulations of the solutions to the boundary value problems and based on the finite element method are also presented. Ongoing research to be reported in the near future and also based on our own experimental work addresses the phenomenon of debonding by stress concentration on the boundary.

Appendix

Figures 10 − 19 and numerical measurements show that the constraint $y_2 \ge 0$ is essentially fulfilled when adding the substrate energy term $A\left(\left(x_2 + u_2(\mathbf{x})\right)^-\right)^2$ of (69) to the energy, with the value chosen of $A = 100000$.
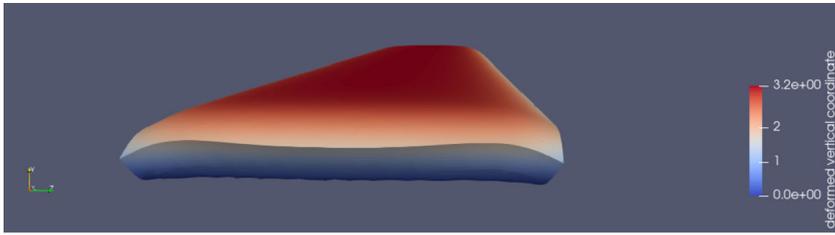
Fig. 10 Left view of the gel at numerical swelling equilibrium, $A = 100000$. The body now remains essentially above the substrate $\{y_2 = 0\}$, as opposed to the situation depicted in Fig. 8 where some points reached heights as low as $y_2 = -0.32$ mm
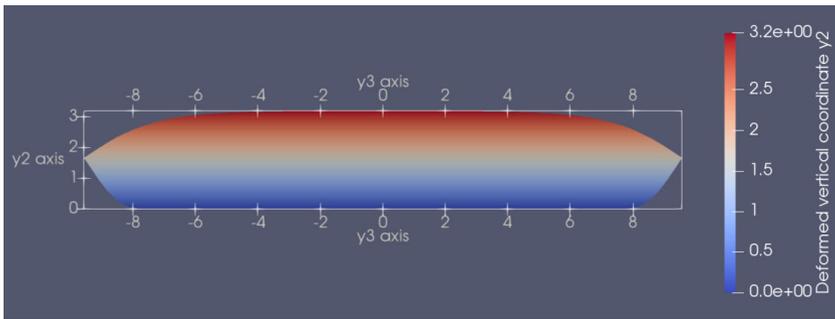
Fig. 11 Cross-section $\{y_1 = 0\}$ of the deformed configuration. Colors indicate the deformed vertical coordinate. Grid lines are drawn at $y_2 = 0$, $y_2 = 3.19$, and $y_3 = \pm 9.56$
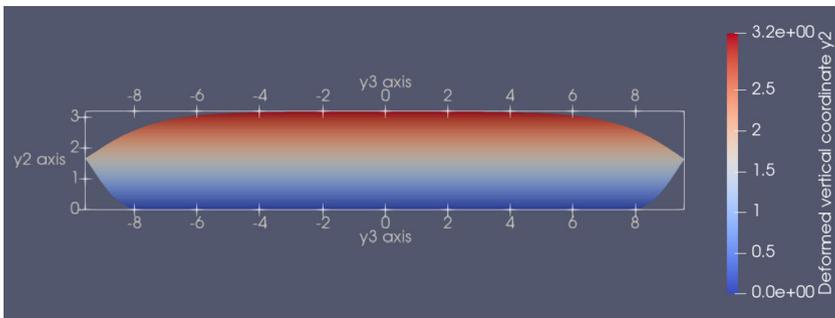
Fig. 12 Cross-section $\{y_1 = 30\}$ of the deformed configuration. Colors indicate the deformed vertical coordinate. Grid lines are drawn at $y_2 = 0$, $y_2 = 3.19$, and $y_3 = \pm 9.56$. There is almost no difference with the slice at $y_1 = 0$
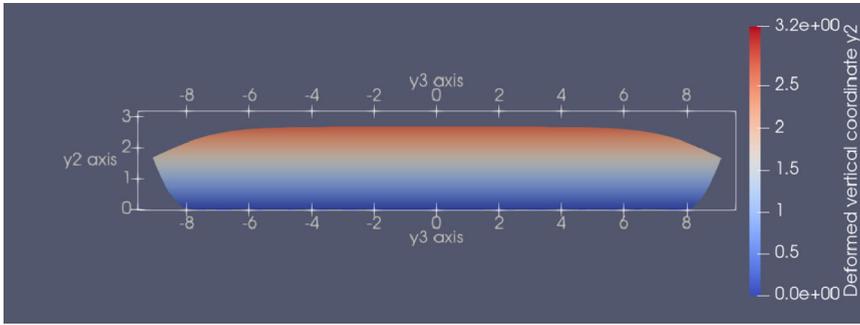
Fig. 13 Cross-section $\{y_1 = 45.1\}$ of the deformed configuration. (The clamped bottom surface ends at $y_1 = 45$, so this slice is taken slightly to the right of the region bonded to the substrate.) Colors indicate the deformed vertical coordinate. Grid lines are drawn at $y_2 = 0$, $y_2 = 3.19$, and $y_3 = \pm 9.56$. Note the smaller tichkness compared to the cross-sections at $y_1 = 0$ and $y_1 = 30$ of Figs. 11–12. This illustrates how the gel, as it swells towards the right, also rotates and falls down a little, which is consistent with the left view of Fig. 10
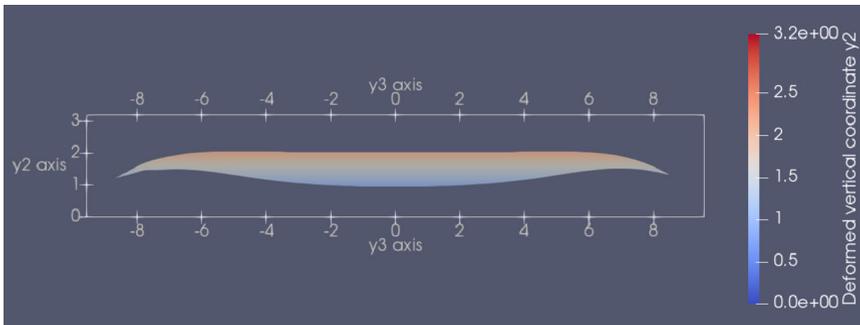
Fig. 14 Cross-section $\{y_1 = 46.5\}$ of the deformed configuration. (The right-most points of the swollen gel are found at $y_1 = 46.99$, $y_3 = 0$.) Colors indicate the deformed vertical coordinate. Grid lines are drawn at $y_2 = 0$, $y_2 = 3.19$, and $y_3 = \pm 9.56$
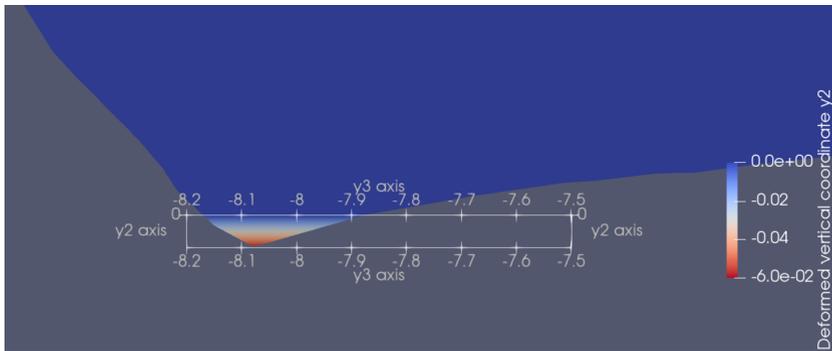
Fig. 15 Cross-section $\{y_1 = 45.57\}$ of the deformed configuration. Colors indicate the deformed vertical coordinate. Grid lines are drawn at $y_2 = -0.06$, $y_2 = 0.00$, $y_3 = -8.2$, and $y_3 = -7.5$. The point in red has the lowest vertical coordinate of the whole deformed gel, at $y_2 = -0.057$ mm. This cross-section is also the one for which the region that violates the constraint $y_2 \geq 0$ of the obstacle problem falls within the largest range of values along the width direction: $-8.17 \leq y_3 \leq -7.87$. Therefore, even in the worst of the cross-sections, the Signorini constraint is violated in a very tiny portion of the gel (in a range of the order of 50 microns). As the prefactor A in the penalization term in (69) tends to infinity, the region where the constraint is violated of not pushing the glass slide downwards is expected to disappear
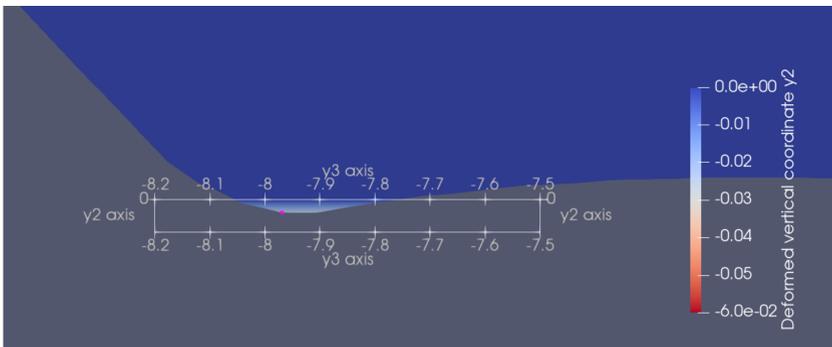
Fig. 16 Cross-section $\{y_1 = 45.4\}$ of the deformed configuration. Colors indicate the deformed vertical co-ordinate. Grid lines are drawn at $y_2 = -0.06$, $y_2 = 0.00$, $y_3 = -8.2$, and $y_3 = -7.5$. The lowest vertical coordinate in this cross-section is $y_2 = -0.02$ mm (the violation of the constraint is already a third of the violation of -0.057 in the worst of the cross-sections, that of Fig. 15). In this corner (at the back and at the bottom of the gel), the effect of pushing downwards the glass slide disappears already at the $\{y_1 = 45.2\}$ cross-section when moving to the left, and at $\{y_1 = 45.8\}$ when moving to the right (the Signorini constraint is violated in a very tiny portion of the gel). As the prefactor $A \to \infty$ in the penalization in (69), the region where the constraint is violated is expected to disappear
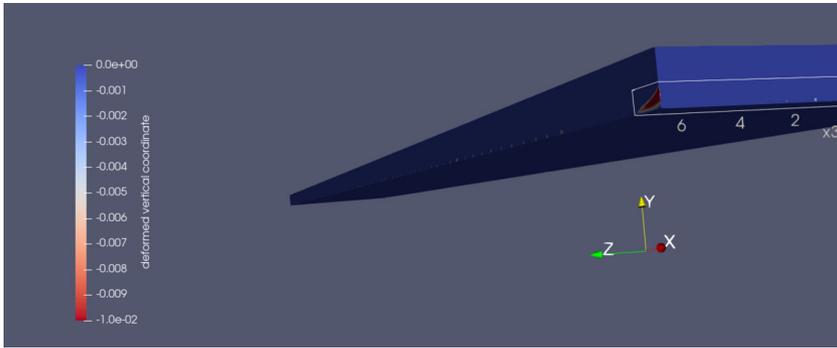
Fig. 17 Localization (view from the front) in the reference configuration of the portion of the gel reaching heights below $\{y_2 = 0\}$ after the deformation. Colors indicate the deformed vertical coordinate (in the range from -0.01 to 0.00 -and higher-). Grid lines are drawn at $x_1 = 43.9$ and $x_2 = 0.7$. As the prefactor $A \to \infty$ in the penalization in (69), the region where the constraint is violated is expected to disappear
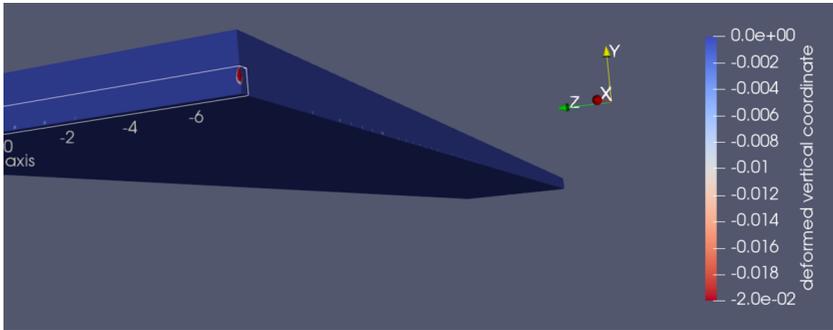
Fig. 18 Localization (view from the back) in the reference configuration of the portion of the gel reaching heights below $\{y_2 = 0\}$ after the deformation. Colors indicate the deformed vertical coordinate (in the range from -0.02 -and lower- to 0.00 -and higher-). Grid lines are drawn at $x_1 = 44.7$, $x_2 = 0.7$, and $x_3 = -7.5$. As the prefactor $A \to \infty$ in the penalization in (69), the region where the constraint is violated is expected to disappear
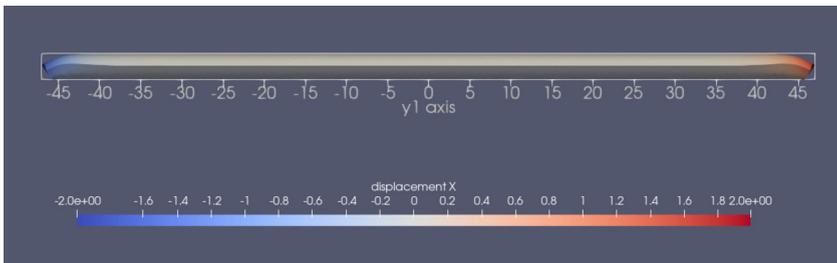
Fig. 19 Main view (from the front) of the swollen gel. Colors indicate the displacement towards the left or the right. Most of the gel exhibits no displacement in this direction. The portion around the corners where the gel bends downwards beyond the $\{y_2 = 0\}$ level is negligible

References

1. Ambrosio, L., Braides, A.: Energies in SBV and variational models in fracture mechanics. In: Cioranescu, D., Damlamian, A., Donato, P. (eds.) Homogenization and Applications to Materials Sciences, pp. 1–22. GAKUTO, Gakkotosho, Tokio, Japan (1997)
2. Arbogast, T., Douglas Jr., J., Hornung, U.: Derivation of the double porosity model of single phase flow via homogenization theory. SIAM J. Math. Anal. **21**, 823–836 (1990)
3. Ball, J.M.: Convexity conditions and existence theorems in nonlinear elasticity. Arch. Ration. Mech. Anal. **63**, 337–403 (1977)
4. Bhalla, A.S., Siegel, R.A.: Mechanistic studies of an autonomously pulsing hydrogel/enzyme system for rhythmic hormone delivery. J. Control. Release **196**, 261–271 (2014)
5. Biot, M.A.: General theory of three-dimensional consolidation. J. Appl. Phys. **12**, 55–164 (1941)
6. Bouklas, N., Huang, R.: Swelling kinetics of polymer gels: comparison of linear and nonlinear theories. Soft Matter **8**, 8194–8203 (2012)
7. Bourdin, B., Francfort, G., Marigo, J.-J.: The variational approach to fracture. J. Elast. **91**, 5–148 (2008)
8. Bowen, R.: Incompressible porous media models by use of the theory of mixtures. Int. J. Eng. Sci. **18**, 1129–1148 (1980)
9. Calderer, M.C., Garavito, C., Henao, D., Tapia, L., Lyu, S.: Gel debonding from a rigid substrate. J. Elast. **141**, 51–73 (2020)
10. Chabaud, B., Calderer, M.C.: Effects of permeability and viscosity in linear polymer gel models. Math. Methods Appl. Sci. **39**, 1395–1409 (2016)
11. Ciarlet, P.: Mathematical Elasticity, vol. 1. North-Holland, Amsterdam (1987)
12. Dacorogna, B.: Direct Methods in the Calculus of Variations. Springer, Berlin (1989)
13. Dhanarajan, A.P., Misra, G.P., Siegel, R.A.: Autonomous chemomechanical oscillations in a hydrogel/enzyme system driven by glucose. J. Phys. Chem. **106**, 8835–8838 (2002)
14. Doi, M.: Soft Matter Physics. Oxford University Press, London (2013)
15. Flory, P.J.: Molecular size distribution in three dimensional polymers. I. Gelation. J. Am. Chem. Soc. **63**, 3083–3090 (1941)
16. Flory, P.J., Rehner, J. Jr.: Statistical mechanics of cross-linked polymer networks I. Rubberlike elasticity. J. Chem. Phys. **11**, 512–520 (1943)
17. Francfort, G., Marigo, J.-J.: Revisiting brittle fracture as an energy minimization problem. J. Mech. Phys. Solids **46**, 1319–1342 (1998)
18. Griffith, A.A.: The phenomena of rupture and flow in solids. Philos. Trans. R. Soc. Lond. Ser. A **221**, 163–198 (1921)
19. Hong, W., Zhao, X., Zhou, J., Suo, Z.: A theory of coupled diffusion and large deformation in polymeric gels. J. Mech. Phys. Solids **56**, 1779–1793 (2008)
20. Huggins, M.L.: Solutions of long chain compounds. J. Chem. Phys. **9**, 440 (1941)
21. Kang, M.K., Huang, R.: Swell-induced surface instability of confined hydrogel layers on substrates. J. Mech. Phys. Solids **58**, 1582–1598 (2010)
22. Misra, G.P., Siegel, R.A.: A new mode of drug delivery: long term autonomous rhythmic hormone release across a hydrogel membrane. J. Control. Release **81**, 1–6 (2002)
23. Mora, T., Boudaoud, A.: Buckling of swelling gels. Eur. Phys. J. E **20**, 119–124 (2006)
24. Mori, Y., Chen, H., Micek, C., Calderer, M.C.: A dynamic model of polyelectrolyte gels. SIAM J. Appl. Math. **73**, 104–133 (2013)
25. Müller, S.: Higher integrability of determinants and weak convergence in L^1. J. Reine Angew. Math. **412**, 20–34 (1990)
26. Pence, T.: On the formulation of boundary value problems with the incompressible constituents constraint in finite deformation poroelasticity. Math. Methods Appl. Sci. **35**, 1756–1783 (2012)
27. Pence, T.J., Tsai, H.: Swelling-induced cavitation of elastic spheres. Math. Mech. Solids **11**, 527–551 (2006)

28. Rognes, M.E., Calderer, M.C., Micek, C.A.: Modelling of and mixed finite element methods for gels in biomedical applications. SIAM J. Appl. Math. **70**, 1305–1329 (2009)
29. Rubinstein, M., Colby, R.H.: Polymer Physics, vol. 23. Oxford University Press, New York (2003)
30. Schöberl, J.: C++ 11 implementation of finite elements in NGSolve. Institute for analysis and scientific computing, vol. 30 (2014)
31. Tanaka, T., Fillmore, D.J.: Kinetics of swelling of gels. J. Chem. Phys. **70**, 1214–1218 (1979)
32. Truesdell, C., Noll, W.: The Non-Linear Field Theories of Mechanics. Springer, Berlin (2004)
33. Weiss, F., Cai, S., Hu, Y., Kang, M.Y., Huang, R., Suo, Z.: Creases and wrinkles on the surface of a swollen gel. J. Appl. Phys. **114**, 073507 (2013)
34. Wineman, A., Rajagopal, K.: Shear induced redistribution of fluid within a uniformly swollen nonlinear elastic cylinder. Int. J. Eng. Sci. **30**, 1583–1595 (1992)
35. Yao, L., Calderer, M.C., Mori, Y., Siegel, R.A.: Rhythmomimetic drug delivery: modeling, analysis, and numerical simulation. SIAM J. Appl. Math. **77**, 565–592 (2017)
36. Yuk, H., Zhang, T., Lin, S., Parada, G.A., Zhao, X.: Tough bonding of hydrogels to diverse non-porous surfaces. Nat. Mater. **15**, 190–196 (2016)

Authors and Affiliations

Sichen Song[1,2] · **Ronald A. Siegel[1]** · **Manuel A. Sánchez[3]** · **M. Carme Calderer[2]** · **Duvan Henao[4,5]**

✉ D. Henao
   duvan.henao@uoh.cl

   S. Song
   song0357@umn.edu

   R.A. Siegel
   siege017@umn.edu

   M.A. Sánchez
   manuel.sanchez@ing.puc.cl

   M.C. Calderer
   calde014@umn.edu

[1] Department of Pharmaceutics, University of Minnesota, Minneapolis, MN 55455, United States

[2] School of Mathematics, University of Minnesota, Minneapolis, MN 55455, United States

[3] Instituto de Ingeniería Matemática y Computacional, Pontificia Universidad Católica de Chile, Santiago, Chile

[4] Facultad de Matemáticas & Instituto de Ingeniería Matemática y Computacional, Pontificia Universidad Católica de Chile, Santiago, Chile

[5] Currently at Instituto de Ciencias de la Ingeniería, Universidad de O'Higgins, Rancagua, Chile